

RESEARCH ARTICLE

10.1002/2016JC011992

Tropical cyclone activity over the Southwest Tropical Indian Ocean

Jessica M. Burns¹, Bulusu Subrahmanyam¹, Ebenezer S. Nyadjro², and V. S. N. Murty³¹School of the Earth Ocean and Environment, University of South Carolina, Columbia, South Carolina, USA, ²Department of Physics, University of New Orleans, New Orleans, Louisiana, USA, ³Council of Scientific and Industrial Research (CSIR)–National Institute of Oceanography Regional Centre, Visakhapatnam, Andhra Pradesh, India

Key Points:

- Positive IOD event in 2012 influenced the number of TC days through downwelling Rossby waves
- 4–5 month lag correlation between Dipole Mode Index and number of TC days in the SWTIO
- Negative correlation between Oceanic Niño Index of positive ENSO phase and TC activity in the SWTIO

Correspondence to:

J. M. Burns,
jburns@geol.sc.edu

Citation:

Burns, J. M., B. Subrahmanyam, E. S. Nyadjro, and V. S. N. Murty (2016), Tropical cyclone activity over the Southwest Tropical Indian Ocean, *J. Geophys. Res. Oceans*, 121, 6389–6402, doi:10.1002/2016JC011992.

Received 24 MAY 2016

Accepted 2 AUG 2016

Accepted article online 8 AUG 2016

Published online 27 AUG 2016

Abstract The Southwest Tropical Indian Ocean (SWTIO) is a key region for air-sea interaction. Tropical cyclones (TCs) regularly form over the SWTIO and subsurface ocean variability influences the cyclogenesis of this region. Tropical cyclone days for this region span from November through April, and peak in January and February during austral summer. Past research provides evidence for more tropical cyclone days over the SWTIO during austral summer (December–June) with a deep thermocline ridge than in austral summer with a shallow thermocline ridge. We have analyzed the Argo temperature data and Hybrid Coordinate Ocean Model (HYCOM) outputs while focusing on the austral summer of 2012/2013 (a positive Indian Ocean Dipole (IOD) year and neutral El Niño Southern Oscillation (ENSO) year) when seven named tropical cyclones developed over the SWTIO region. This study reveals that the climatic events like the IOD and ENSO influence the cyclonic activity and number of TC days over the SWTIO. We ascertain that the IOD events have linkages with the Barrier Layer Thickness (BLT) in the SWTIO region through propagating Rossby waves, and further show that the BLT variability influences the cyclonic activity in this region.

1. Introduction

In the Southwest Tropical Indian Ocean (SWTIO), tropical cyclone season is from November through April. On an average, about 15 tropical storms form over the SWTIO and move across the Indian Ocean basin, and ultimately pose a major threat to the Indian Ocean rim countries, especially in eastern Africa. A recent report for the 2012/2013 TC season [RSMC, 2015] suggested that, although only one TC crossed over land, many of the cyclones were close enough to affect inhabited lands, and *Haruna* even claimed victims on the island of Madagascar.

Over the SWTIO, most of the tropical storms that later develop into tropical cyclones (TCs) are formed between the latitudinal belt of 5°S–10°S [Vialard *et al.*, 2009]. The Seychelles-Chagos Thermocline Ridge (SCTR), bounded by 55°E–65°E and 5°S–12°S, overlaps this active tropical cyclone band. Although the main upwelling region of the SCTR is between 55°–65°E and 5°–12°S, the upwelling extends as far east as 80°E. This SCTR region is an important region for air-sea interaction and is unique in that the variability of the subsurface ocean processes can influence the cyclogenesis [Hermes and Reason, 2009b]. The strong connection between the depth of the thermocline and Sea Surface Temperature (SST) in the SCTR region, and its proximity to the equator where the atmosphere is already sensitive to variations in SST, suggests that the SCTR is an important region for not only air-sea interaction but also variations in tropical circulations [Manola *et al.*, 2015]. Variations in the SCTR affect cyclogenesis over the SWTIO because the thermocline is shallowest from December to June (austral summer), a period that overlaps with the cyclone season [Xie *et al.*, 2002; Hermes and Reason, 2009a; Manola *et al.*, 2015]. Cyclogenesis over this region is also impacted by atmospheric stability, which in turn is influenced by SST [Annamalai *et al.*, 2003; Hermes and Reason, 2009a]. Hermes and Reason [2009b] provided the evidence for more number of observed tropical cyclone days over SWTIO during austral summers of deep thermocline ridge than those with a shallow thermocline ridge. The reason is that when the ridge is dynamically made-up of a deeper mixed layer, it experiences heightened SST, which is a key ingredient for cyclogenesis [Hermes and Reason, 2009b]. Additionally, the deep thermocline suppresses the feedback to the SST as upwelling of cooler subsurface waters is restrained. The inhibition of mixing at the base of mixed layer prevents the cooler waters from mixing to the surface and lowering of SST. During austral summer, the SCTR features a SST range between 28.5°C and 30°C, which

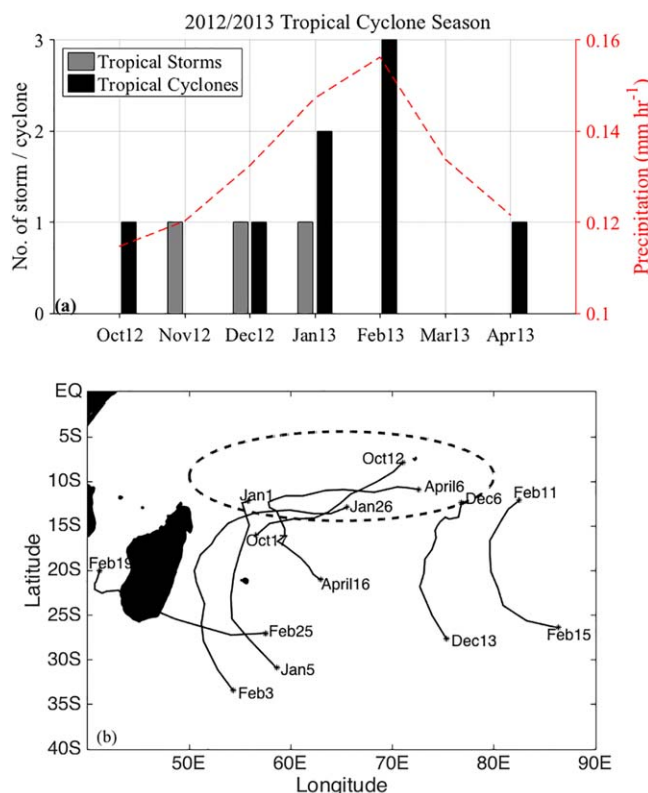


Figure 1. (a) Distributions of tropical storms and named tropical cyclones during 2012–2013 Tropical Cyclone Season in the Southwest Tropical Indian Ocean basin. The dashed red line represents precipitation rate (mm h⁻¹). (b) The 2012/2013 cyclone season seven named tropical cyclone tracks in the SWTIO. The black dashed circle is the SCTR region.

makes the atmosphere sensitive to small changes in SST [Vialard *et al.*, 2009]. This SST range is unusual for a quasi-permanent upwelling region. Most upwelling regions similar to the SCTR (e.g., eastern tropical Pacific) have SSTs much below 28.5°C resulting from cold thermocline waters brought to the surface under the influence of anticyclonic wind stress curl field during austral summer [McCreary *et al.*, 1993]. However, on a seasonal time scale, the vertical advection by way of upwelling has little effect on the mixed layer temperature or SSTs so during upwelling times the colder water below does not significantly cool the water at the surface through vertical advection [Halkides and Lee, 2009].

The Barrier Layer (BL) is defined as the layer between the thermocline and the halocline. BL formation is an important parameter for surface heat exchange and thus heat content in the ocean. The stratification due to the vertical distribution of salinity may affect heat exchange between the ocean and atmosphere, thus affecting cyclogenesis. Balaguru *et al.* [2012]

demonstrated that in parts of the tropical Pacific, Atlantic, and the northern Indian Ocean basins, salinity stratified BLs in the upper ocean influence TC intensification. The same study also demonstrated that in tropical ocean basins, typically, the intensification rate of TCs is about 50% higher over the BL regions than in regions without BLs. The occurrence of a salt-stratified BL causes stratification that reduces entrainment cooling from below the mixed layer. This process delays development of a cold wake needed to provide a negative feedback on the enthalpy flux to the TC.

This study focuses on austral summer of 2012/2013 when seven named TCs developed over the SWTIO during cyclone season, including the occurrence of the intense TC ‘Anais’, preceding the typical tropical cyclone season, in October. Usually, the cyclone season in the SWTIO does not begin until November and there are only on average 5 named cyclones and 10 tropical storms per season [Vialard *et al.*, 2009]. We explore the impacts of IOD and ENSO events on the formation of TCs and their intensification in the SWTIO region. The archived data of tropical storms and their paths from 1982 through 2013 were downloaded from Unisys Weather and Typhoon Warning Center (http://www.usno.navy.mil/NOOC/nmfc-ph/RSS/jtwc/best_tracks/shindex.php).

Primarily, Argo observations of salinity and temperature along with HYCOM simulations are used to examine the influence of the SWTIO region on cyclone formation and intensity in this region. All analyses are performed on the extended SCTR upwelling region (55°–80°E and 5°–12°S), unless otherwise specified. Correlating the dynamics of the SCTR region with tropical cyclone activity will hopefully provide an insight to cyclone formation and intensity in this region and ultimately lead to more accurate cyclone intensity and track forecasts.

The rest of the paper is organized into four main sections. Section 2 describes the data used and methodology adopted. Section 3 entails the results and discussions; including a discussion of cyclonic activity over the SWTIO and the role of Rossby waves, IOD, and ENSO on TC activity. Finally, a summary and conclusion of the study is provided in section 4.

Table 1. 2012/2013 Tropical Cyclone Dates, Times, Location, Intensity, and Daily Barrier Layer Thickness Along Cyclone Track

TC	Date	Time (UTC)	Location	Intensity (kt)	BLT (m)	TC	Date	Time (UTC)	Location	Intensity (kt)	BLT (m)
FELLENG [2013]	1/30	0000	14.7S, 53.8E	105	21		2/12	1200	16.6S, 79.6E	75	9.5
	1/30	0600	15S, 53.3E	110			2/12	1800	17.2S, 79.6E	80	
	1/30	1200	16.2S, 52.6E	115		GINO [2013]	2/13	0000	18.3S, 79.6E	90	
	1/30	1800	16.9S, 52.2E	105			2/13	0600	18.9S, 79.4E	90	
CLAUDIA [2012]	1/31	0000	17.7S, 52E	95	21.8		2/13	1200	20.1S, 79.7E	85	18.7
	12/8	0600	14.3S, 75E	90	16.9		2/13	1800	21S, 80.2E	85	
	12/8	1200	14.5S, 74.7E	100			4/10	0000	11.7S, 58.7E	65	
	12/8	1800	14.4S, 74.4E	110			4/10	0600	12S, 58.4E	70	2.2
	12/9	0000	15S, 74.4E	105			4/10	1200	12.1S, 58E	75	
	12/9	0600	15.1S, 74.2E	105	18.1		4/10	1800	12.3S, 57.8E	85	
	12/9	1200	15.5S, 74.2E	100			4/11	0000	12.6S, 58.1E	80	
	12/9	1800	15.7S, 74.2E	115			4/11	0600	12.9S, 57.9E	75	3
	12/10	0000	16.3S, 74.3E	105			4/11	1200	13S, 58.2E	65	
	12/10	0600	16.8S, 74E	105	6	IMELDA [2013]	4/11	1800	13.3S, 58.6E	55	
	12/10	1200	17.6S, 73.9E	105			4/12	0600	14.1S, 58.9E	45	2.3
		12/10	1800	18S, 73.6E	100			4/12	1200	14.5S, 59.1E	40
	12/11	0000	18.7S, 73.2E	90			4/12	1800	15.3S, 59.4E	35	
ANAIS [2012]	10/14	0600	11S, 66.2E	85	42.1		4/13	0000	15.7S, 59.6E	35	
	10/14	1200	11.4S, 65.9E	105			4/13	0600	16.1S, 59.4E	35	2.8
	10/14	1800	11.8S, 65.3E	105			4/13	1200	16.5S, 58.9E	45	
	10/15	0000	12.4S, 64.9E	100			4/13	1800	16.7S, 58.7E	50	
	10/15	0600	12.8S, 64.4E	110	20.7		4/14	0000	16.9S, 58.5E	55	
	10/15	1200	13.4S, 63.7E	100			4/14	0600	17.2S, 59.4E	60	3.8
HARUNA [2013]	10/15	1800	13.4S, 63E	95			4/14	1200	17.6S, 59.9E	65	
	2/20	1200	22.1S, 40.7E	70	6.8		4/14	1800	18.6S, 61E	75	
	2/20	1800	22.2S, 41.1E	90			4/15	0000	18.7S, 61.4E	75	
	2/21	0000	22.5S, 41.4E	95			1/3	0600	20.3S, 54.4E	65	8.9
	2/21	0600	22.4S, 41.7E	100	4.9		1/3	1200	21.5S, 54.3E	70	
	2/21	1200	22.3S, 41.9E	100		DUMILE [2013]	1/3	1800	22.9S, 54.1E	70	
	2/21	1800	22.1S, 42.3E	90			1/4	0000	24.2S, 54.4E	75	
	2/22	0000	22.2S, 43E	90			1/4	0600	25.4S, 54.2E	70	12.3
2/22	0600	22.3S, 43.5E	85	6		1/4	1200	26.5S, 54.7E	65		

2. Data and Methodology

2.1. Data Sources

The tropical cyclone days and their location data and surface winds data used in this study were downloaded from the Joint Typhoon Warning Center (JTWC) best track data set for the Southern Hemisphere [Chu *et al.*, 2002]. Additionally, track information and hurricane data for the 2012/2013 SWTIO TC season were obtained from Unisys Weather and the National Aeronautics and Space Administration's (NASA) past years Hurricane/Tropical Cyclone news archive. Whenever the JTWC issues a warning, the Regional and Mesoscale Meteorology Branch (RAMMB) estimates TC intensities based on winds and temperature every 6 h [Sampson and Schrader, 2000]. Only the TCs over the SWTIO basin (i.e., 40–90°E and 0–40°S) were considered in this study. In addition, the World Meteorological Organization (WMO) defines tropical cyclones in the SWTIO as having maximum sustained winds near the center exceeding 33 ms^{-1} , therefore only cases that met this criterion were considered for estimating the TC days for the purpose of this study. Oceanic Niño Index (ONI) region 3.4 values were obtained from the National Weather Service Climate Prediction Center [Wolter and Timlin, 1993, 1998]. Dipole Mode Index (DMI), a measure of IOD intensity, data were obtained from *The State of the Ocean Climate* webpage (stateoftheocean.osmc.noaa.gov/sur/ind/dmi.php). The DMI is defined as the difference in SST anomaly between the south-eastern Indian Ocean (90° E–110° E and 10° S–0°) and the western Indian Ocean (50° E–70° E and 10° S–10° N) [Saji *et al.*, 1999].

Argo floats drift within the ocean and typically retrieves salinity and temperature in the water column. The Argo SST data were obtained from the Asian Pacific Research Center (APDRC). APDRC takes the raw data from the Argo profiles and grids them into $1^\circ \times 1^\circ$ resolutions using optimal interpolation. APDRC also applies the raw data horizontal binning and vertical interpolation, where the data are interpolated onto standard depth levels.

In this study, we used a data assimilative version of the HYbrid Coordinate Ocean Model (HYCOM). HYCOM is extensively described in Bleck [2002], Chassignet *et al.* [2003], and Metzger *et al.* [2014]. The model has a

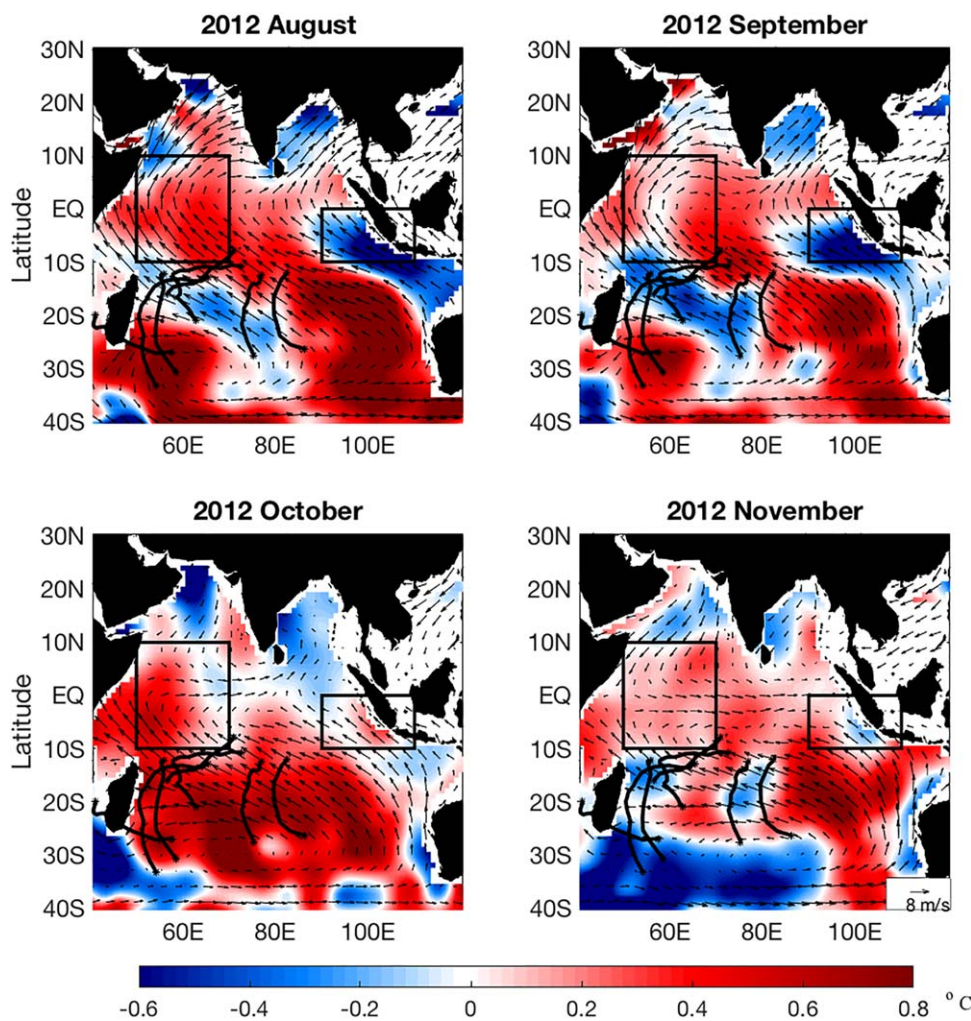


Figure 2. Argo monthly interannual SST anomalies for August–November 2012 using Argo data for a period of 2005–2014. Monthly mean ECMWF interannual wind anomalies are superimposed. Wind interannual anomalies were calculated with a base period of 1992–2013. The black boxes denote the south-eastern IO (90° E–110° E and 10° S–0°) and the western IO (50° E–70° E and 10° S–10° N), the regions of SST anomalies used to define the dipole mode index [Saji et al., 1999]. The black lines are the 2012/2013 TC season TC tracks.

nominal horizontal resolution of $1/12^\circ$ and 41 hybrid layers in the vertical. It is isopycnal in the open stratified ocean, and makes a smooth transition to a terrain following (σ) coordinate in coastal waters using the layered continuity equation. The HYCOM system uses the Navy Coupled Ocean Data Assimilation (NCODA) system [Cummings and Smedstad, 2013] for data assimilation. NCODA uses the model forecast as a first guess in a three-dimensional variational scheme and assimilates available satellite altimeter observations, satellite and in-situ SST as well as available in-situ vertical temperature and salinity profiles from CTDs, Argo floats and moored buoys. The outputs of profiles of salinity and temperature were interpolated to calculate the mixed layer depth (MLD), isothermal layer depth (ILD), and barrier layer thickness (BLT).

The European Centre for Medium-Range Weather Forecasts (ECMWF) provides an archive of meteorological data. In this study, we utilized the ECMWF’s monthly mean 10 m wind and monthly mean 850 hPa relative vorticity. In addition, we used the monthly mean 700 hPa and 500 hPa relative humidity (R.H.), monthly mean 850 hPa and 500 hPa air temperature, and monthly mean horizontal and meridional components of the 200 hPa and 850 hPa wind vectors to compute atmospheric parameters known to influence cyclogenesis (discussed in the methodology section).

Daily sea surface height anomaly (SSHA) data for 2010–2015 were obtained from Archiving Validation and Interpretation of Satellite Oceanographic data (AVISO) (<http://www.aviso.oceanobs.com>) [Duquet et al. 2000].

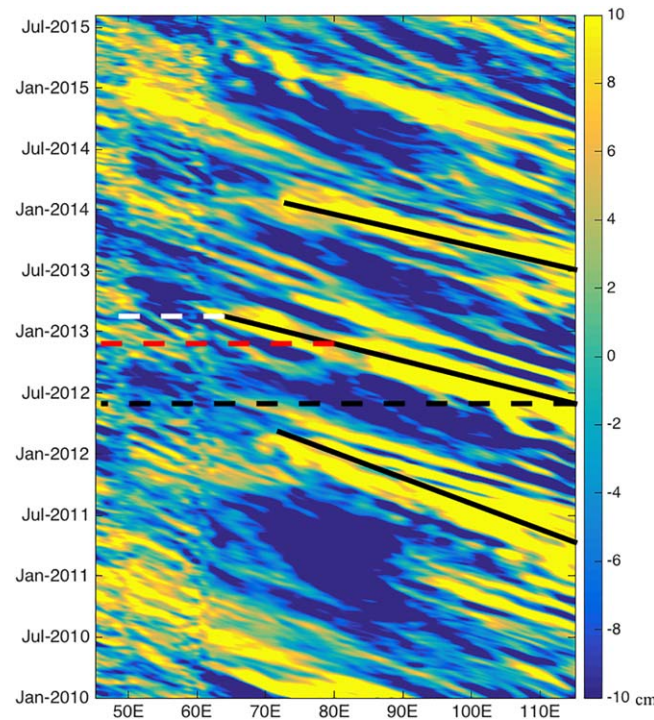


Figure 3. Hövmöller (time versus longitude) plot of AVISO sea surface height anomalies (SSHA) at 12°S during 2010–2015. Estimations of the Rossby wave propagations are represented with black lines. The dashed red and white lines are when the Rossby wave reaches the SCTR and the SCTR main upwelling region respectively. The estimated propagation speeds corresponding to the top, middle, and bottom Rossby waves denoted with black respectively are 27 cm s⁻¹, 25 cm s⁻¹, and 17 cm s⁻¹.

This product, a representation of SSH relative to the 1993–2012 mean sea level, is produced by merging altimetry measurements from several satellites including Ocean Topography Experiment (TOPEX)/Poseidon, Jason, European Remote Sensing Satellite (ERS-1/2), and Environmental Satellite (Envisat). In this study, the AVISO altimetry data were used to observe Rossby wave propagation across the SWTIO basin.

Monthly precipitation (P) data were obtained from the Tropical Rainfall Measuring Mission (TRMM) [Hoffman *et al.*, 2007] product 3B42 version 7. The data are produced from a combination of rain gauge and satellite data and are available on a 0.25° × 0.25° grid.

2.2. Methodology

To find the MLD, we used the variable density criterion method as described in Felton *et al.* [2013] where Δσ is the density change from the surface to the MLD base:

$$\Delta\sigma = \sigma_t(T_0 + \Delta T, S_0, P_0) - \sigma_t(T_0, S_0, P_0) \tag{1}$$

The term $\sigma_t(T_0 + \Delta T, S_0, P_0)$ accounts for the presence of thermal inversion since it is the density equal to the change in temperature from the surface while salinity and pressure are constant as at sea surface. The $\sigma_t(T_0, S_0, P_0)$ term is the surface σ_t value. Each location was searched to find the depth where the density changed by an amount equivalent to a change in temperature of 0.5° C from the surface, and this depth was then defined as the MLD.

For both MLD and ILD, linear interpolations of the HYCOM data were used to obtain the approximate depth. The ILD is defined as the depth where the temperature is ±0.5°C from the surface temperature ($T_z - T_o = 0.5$), where T_o is the surface temperature and T_z is the temperature at depth, z. The BLT is then calculated by taking the difference between the ILD and MLD (BLT=ILD-MLD).

Gray [1968, 1979] proposed vertical wind shear, midtropospheric R.H., and midtropospheric thermal instability to be among the atmospheric parameters influencing cyclogenesis. The midtropospheric R.H. is computed by taking the difference between the R.H. at 700 hPa and 500 hPa (midtropospheric R.H. (%) = R.H._{700 hPa} - R.H._{500 hPa}). The midtropospheric instability is computed as the air temperature at 850 hPa minus the air temperature at 500 hPa (midtropospheric instability = $T_{850 \text{ hPa}} - T_{500 \text{ hPa}}$). The vertical wind shear (m s⁻¹) is computed using the vector wind speed at 200 hPa and 850 hPa where u is the zonal component of the wind speed and v is the meridional component of the wind speed:

$$\text{Vertical wind shear (ms}^{-1}\text{)} = \sqrt{(U_{200 \text{ hPa}} - U_{850 \text{ hPa}})^2 + (V_{200 \text{ hPa}} - V_{850 \text{ hPa}})^2}$$

To examine the relationship between ENSO and number of TCs and ENSO and number of TC days in the SWTIO from 1981 to 2013 we needed to standardize the data for the different phases of ENSO. To do this we took the mean number of TCs during neutral years, subtracted out the long-term mean of TCs and divided by the standard deviation. We did this for each phase of ENSO for both TCs and TC days.

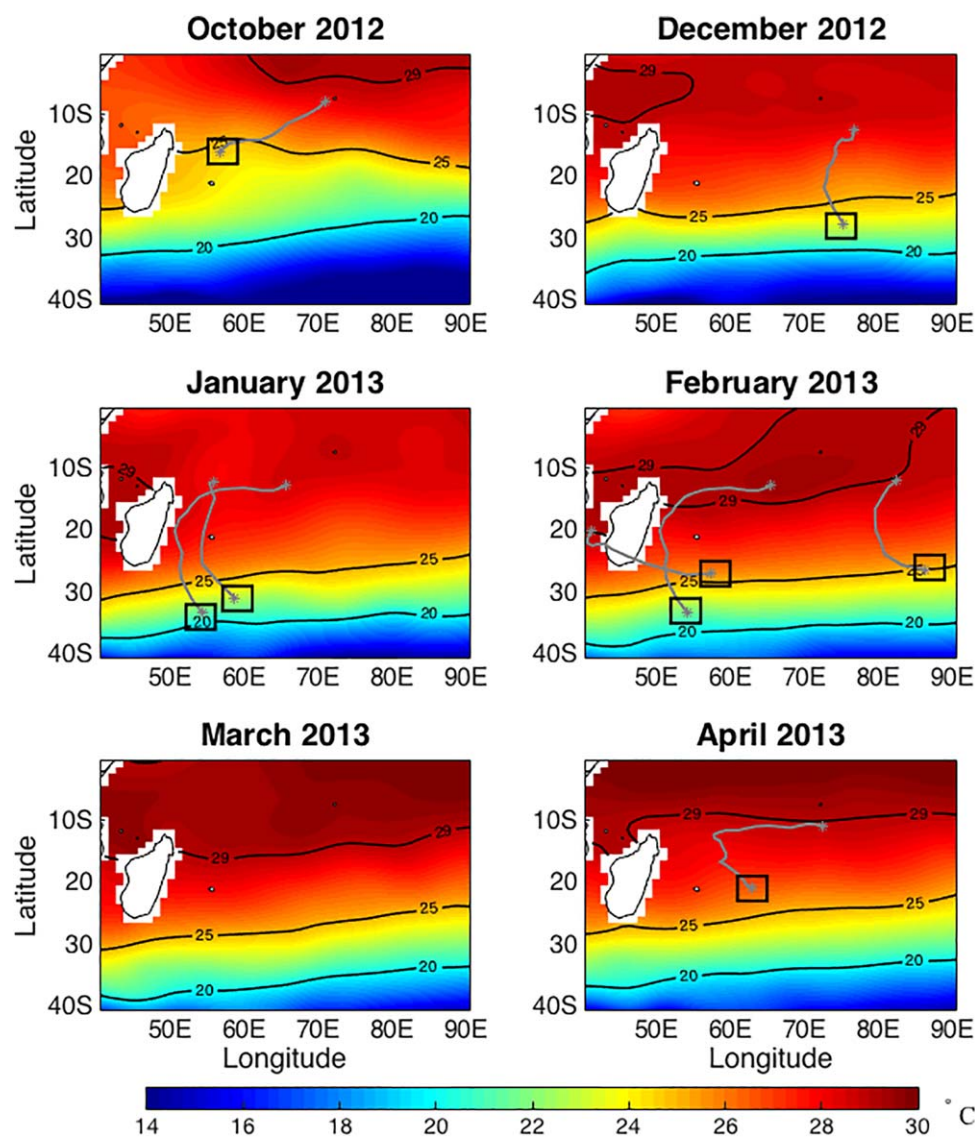


Figure 4. Monthly averages of Argo SST with cyclones tracks (gray) for each month. The black box is where the tropical storms died out. 20°C, 25°C, and 29°C isotherms are contoured in black.

3. Results and Discussion

3.1. 2012/2013 Cyclonic Activity in the Southwest Tropical Indian Ocean

Tropical cyclone days for the SWTIO span from November through April, with an average of 15 tropical storms and named cyclones that track across the basin. In the 2012/2013 season, there were seven named tropical cyclones (Figure 1a; *Anais* (October 2012), *Claudia* (December 2012), *Dumile* (January 2013), *Felleng* (January 2013), *Gino* (February 2013), *Haruna* (February 2013), and *Imelda* (April 2013)). The tracks of these cyclones are displayed in Figure 1b. All the cyclones started within a few degrees of the equator in the SCTR region or just south of the region and traveled poleward. The most intense cyclone was at the end of January going into February with the cyclone in December and the cyclone in October followed closely behind (Table 1). The 2012 positive IOD event may have influenced the intensity and variability of these TCs through the propagation of downwelling Rossby waves.

Generally, winds north of the equator are westerly while winds south of the equator are easterly. However, during positive IOD years, the normal equatorial westerly winds weaken and eventually reverse direction to easterly. This wind anomaly and associated Ekman pumping generate off-equatorial Rossby waves that

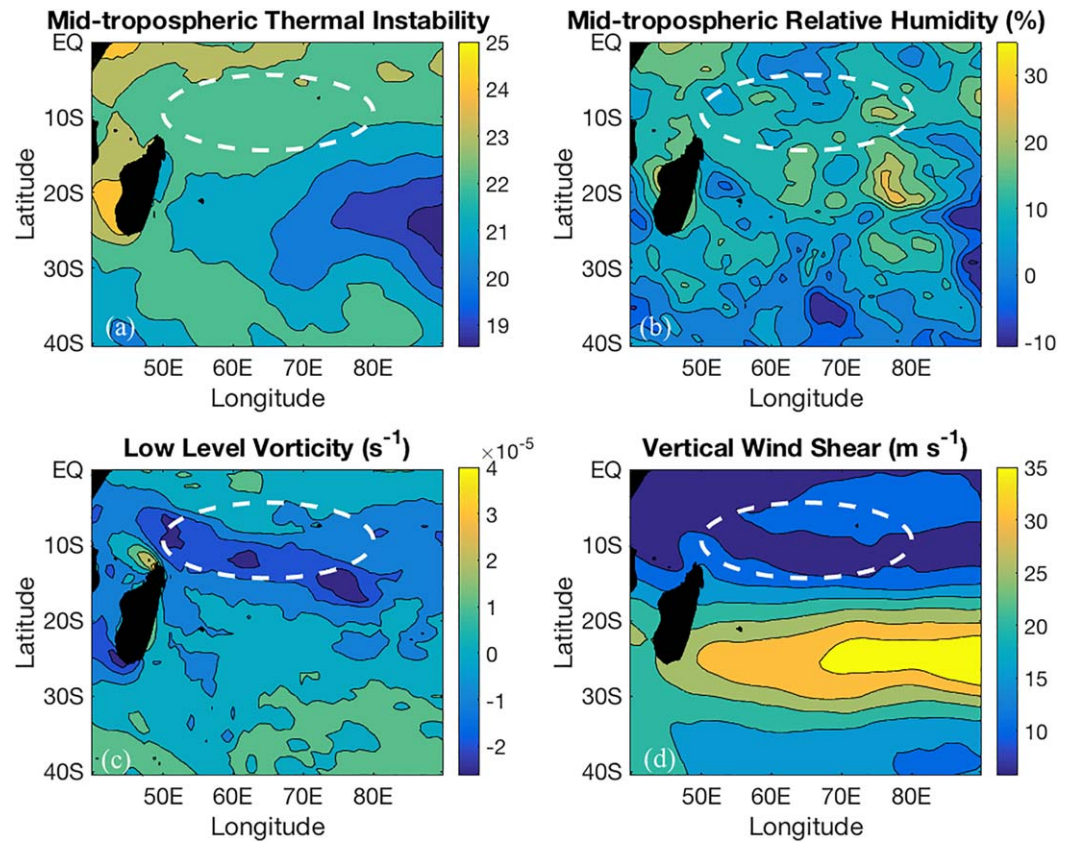


Figure 5. Distribution of various cyclogenesis parameters in the SWIO for March 2013—(a) Midtropospheric thermal instability, (b) midtropospheric relative humidity, (c) low level vorticity, and (d) vertical wind shear. The dashed white oval is the SCTR region.

propagate westward and act to deepen the thermocline; thus warming the SST in the western part of the Indian Ocean [Gnanaseelan et al., 2008; Chowdary et al., 2009]. Figure 2 shows the wind anomalies plotted over SST anomalies for the peak months during the 2012 positive IOD. This IOD event is unique in that the IOD peaked in August and September (Figure 2). The early peak may be attributed to the quick weakening and reversal of the westerly trade winds north of the equator. Strong westerlies near the equator can create unfavorable conditions for the negative dipole [Vinayachandran et al., 2009]. However, if the westerlies

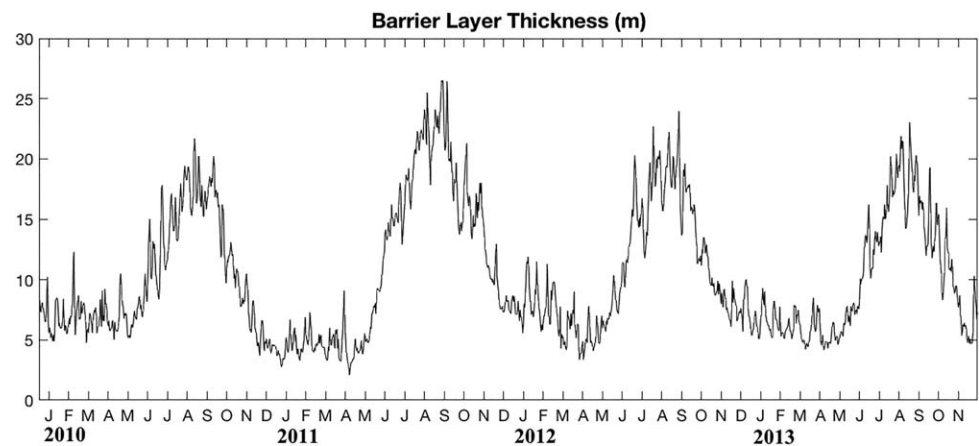


Figure 6. Time series of daily variation of Barrier Layer Thickness (BLT in meters) averaged over the entire SCTR upwelling region (55°–85°E and 5°–12°S) for years 2010–2013.

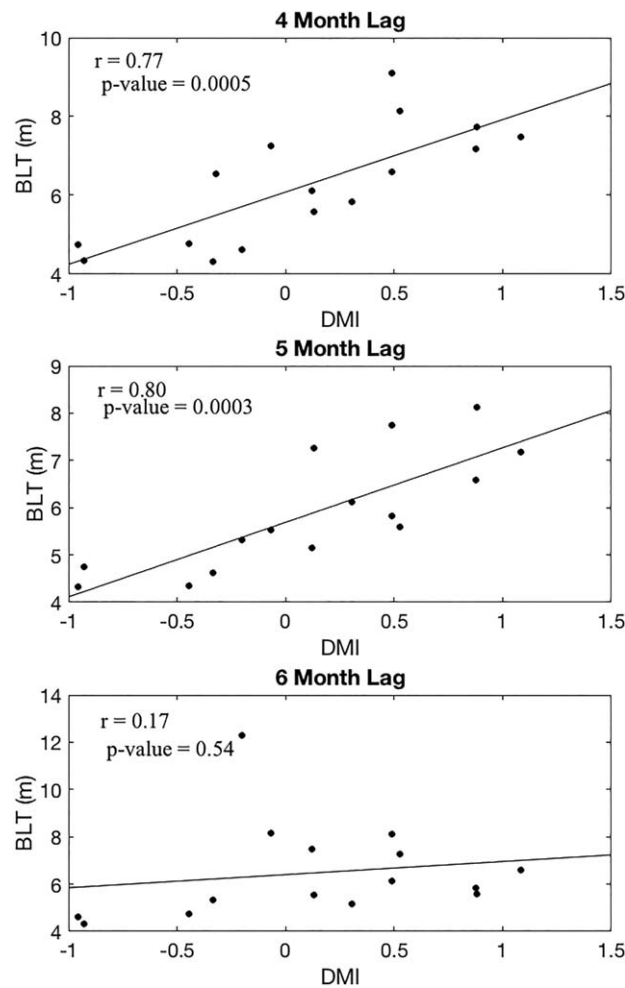


Figure 7. Scatter plots (with data from years 2010 to 2013) showing the relationship between Dipole Mode Index (DMI) during peak IOD months and the BLT in the SCTR region with a lag of 4, 5, and 6 months.

waves reach the SCTR region and deepen the thermocline heat content increases in the western part of the Indian Ocean, thus supporting TC development. According to the National Oceanographic Data Center (NODC) [Levitus *et al.*, 2012] the mean 0–700 m layer total heat content (THC) in the South Indian Ocean for the months of July–September 2012 was 2.6×10^{22} J. For the months of October–December 2012 the THC was 3.2×10^{22} J. THC for January–March 2013 was 3.4×10^{22} J, and for April–June 2013 the THC decreased again to 2.3×10^{22} J. The spike in total heat content during the October–March period agrees with the Rossby waves propagating westward across the Indian Ocean basin and reaching the 60–80°E longitude range within 4–6 months.

Figure 4 shows that all of the cyclones developed in areas of SST of approximately 28°C and died in areas of SST varying between 24° and 26°C. Unlike other seasons, March had no tropical cyclone activity. Gray [1968] proposed many preconditions of oceanic and atmospheric parameters for the cyclogenesis including a threshold of SST above 26°C, high low-level relative vorticity, low vertical wind shear, high midtropospheric relative humidity, and high midtropospheric thermal instability. Since SSTs in this SCTR region were warm enough during March 2013 (Figure 4), the absence of any tropical cyclone activity during this month is likely a result of an unfavorable atmospheric condition. During March 2013, there was high vertical wind shear (Figure 5), which might have torn any developing storm apart. In addition, there was also low relative humidity (Figure 5), thus dry layers could have also suppressed any cyclone development.

quickly weakened, earlier than usual, this would allow the negative dipole to form and peak earlier than usual off the west coast of Sumatra. In Figure 2 it is seen that by August 2012 the trade winds immediately north of the equator were already anomalously easterly and beginning to weaken and return to their normal westerly flow. As these winds further weaken and reverse back, the thermocline deepens [Vinayachandran *et al.*, 2009], and the negative dipole decays. Since the IOD had an early peak, the region of the 2012/2013 TC cyclone tracks in the SWTIO experienced warmer SST earlier than usual (Figure 2) in the month of October. As a result, we see TC occurrence earlier (October) than the typical start of the TC season (November), and an earlier peak in TC season as well, with 4 of the 7 cyclones of the 2012/2013 season occurring in the months of January and February.

For the 2012/2013 TC season, most of the TCs formed east of the major upwelling zone of the SCTR, in the 60–80°E longitude range. In Figure 3, we see the Rossby wave enters the SWTIO in mid-2012 (dashed black line). The Rossby wave propagates at an estimated speed of 25 cm s^{-1} . With this speed, the high SSH anomalies reach the 60–80°E longitude range by late 2012 and early 2013 (dashed red and white lines), coinciding with higher TC activity. As the Rossby

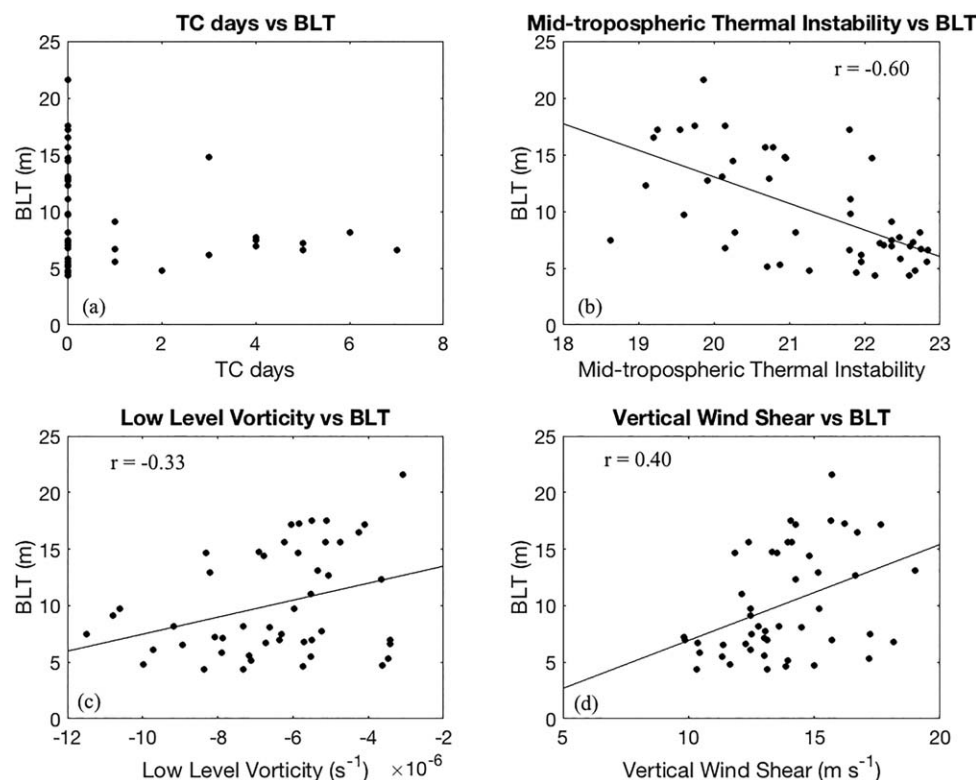


Figure 8. Scatter plots (with data from years 2010 to 2013) showing the relationships (a) between BLT (in the SCTR region) and TC days, (b) between BLT and midtropospheric Thermal Instability, (c) between BLT and Low level vorticity, and (d) between BLT and vertical wind shear. The best fit line is plotted in black.

3.2. Evolution of Barrier Layer and Mixed Layer Dynamics

Salinity stratification in the ocean results in a difference between the ILD and MLD, creating a BL, which is important in regulating surface heat exchanges [Felton *et al.*, 2014]. The thickness of this BL varies seasonally in this region (Figure 6). Since the BL is important in regulating surface heat exchanges, it also may play a role in the formation of TCs in the SWTIO. As TCs pass over BLs, SST cooling decreased due to reduced efficiency in vertical mixing [Balaguru *et al.*, 2012]. This reduction in SST cooling then strengthens TCs through changes in air-sea heat transfers.

Chowdary *et al.* [2009] explains that Rossby wave induced surface warming results from downwelling Rossby waves pushing the thermocline downward resulting in a deeper thermocline thus creating a thicker BL and contributing to surface warming. Since the IOD events result in the propagation of upwelling and downwelling Rossby waves, they would thus influence the BLs. Figure 7 shows the relationship between the DMI of each month during peak IOD (August–December) and the BLT 4 months, 5 months, and 6 months later. Significant correlation exists up to 4–5 months (not significant at 6 month lag, Figure 7). This suggests that the impact of the IOD on BLT extends beyond the peak months of the IOD, up to about 5 months (i.e., into the year after the IOD events). This is plausible as, for example, during the peak of positive IOD events, the warming SST increases convective activities which induces more rainfall, increases stratification, strengthens Surface Temperature Anomalies (SSTA) and further enhances the BLT. Additionally, the higher SSTAs feedback to strengthen the zonal winds which further enhances the downwelling during these events.

The BL may inhibit entrainment and maintain higher SSTs favoring cyclogenesis, but atmospheric conditions are also very important for cyclogenesis. Figure 8 examines how BLT may correlate to atmospheric conditions important for cyclogenesis over a 4 year period. During, January 2010 to December 2013 the thicker the BLT is, the higher the vertical wind shear is. This would result in a competition of favorable conditions for cyclogenesis since thicker BLs may help inhibit entrainment and maintain high SSTs but

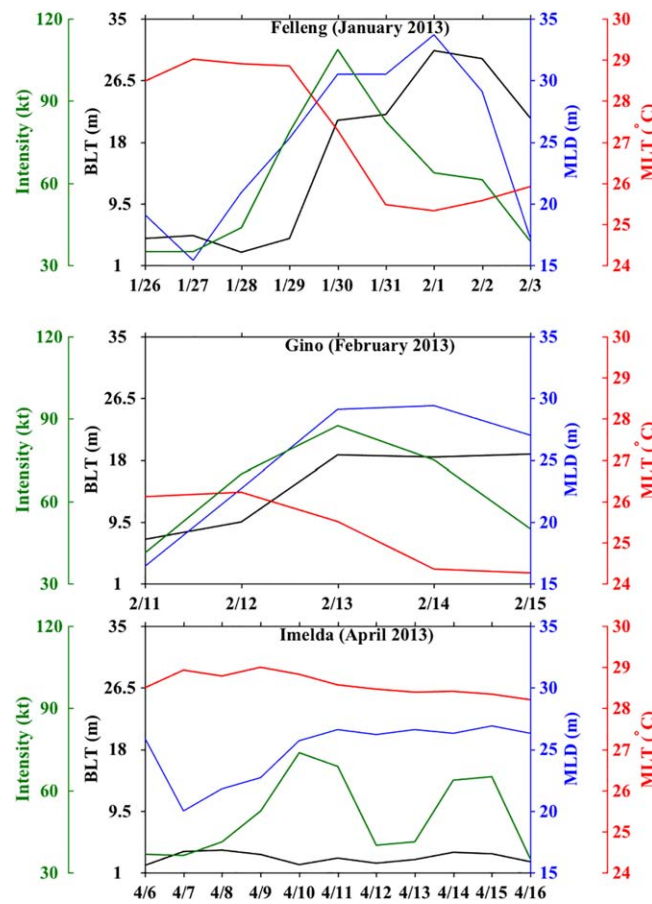


Figure 9. Evolution of MLD (blue line), MLT (red line) and BLT (black line) spatially averaged over the entire cyclone track during the three tropical cyclones (out of the seven cyclones) in 2012/2013 cyclone season based on the HYCOM. The intensity of each cyclone is plotted in green.

high vertical wind shear negatively influences cyclogenesis by tearing the storm apart. The midtropospheric stability would also result in cyclogenesis competition during these years. For TC formation, higher thermal instability in the midtroposphere is essential, but associated with high instability is a lower BLT during 2010–2013. With regard to vorticity in atmospheric winds, the relationship between low level vorticity and BLT seems to be more variable (Figure 8).

Results from *Mainelli et al.* [2008] support the idea that the upper ocean thermal structure is important in TC intensity changes. While IOD events and Rossby waves may influence BLs, feedback between the storm and the BL may also exist. Figure 9 examines the subsurface ocean structure by showing the evolution of MLD (blue line), the mixed layer temperature (MLT, red line) and the BLT (black line) for the three cyclones out of the seven TCs in 2012/2013. In the first two cases (*Felleng* and *Gino*), the BL thickens along the tracks. In the case of *Imelda*, we do not see this happening (Figure 9). The TC *Imelda* was a long lasting storm and instead of traveling southward,

the storm tracked westward for a while, before turning southward. Therefore, most of the storm track (where BLT is spatially averaged) was in the SCTR upwelling region where subsurface dynamics differ.

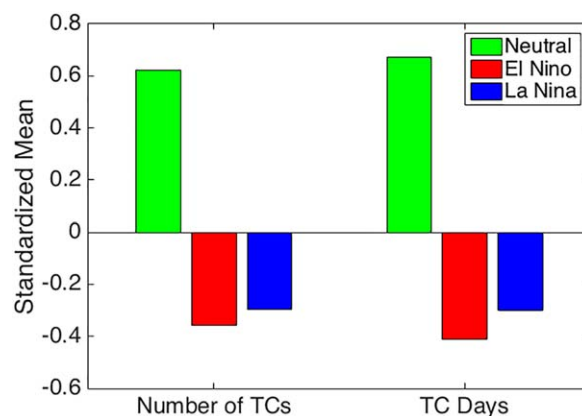


Figure 10. Relationship between ENSO and number of TCs and ENSO and number of TC days in the SWTIO from 1981 to 2013. The y axis represents how many standard deviations the mean number of TCs and TC days for each ENSO phase is above and below the long-term mean.

In all three cases of TCs, we observe something different with regard to the BLT and intensity of the cyclone. In the first two cases (*Felleng* and *Gino*), at the start of the cyclones, BL thickens along the tracks and at the same time the TC intensity increases. During *Felleng*, as its intensity peaks, we see a short leveling of the BLT then and increase again. In the case of *Gino*, we just see a leveling of the BLT after the storm peaks in intensity. In the case of *Imelda* the BLT remains constant throughout the cyclone life and we observe 2 peaks in intensity. The large variability between these results suggests that the BLT alone does not significantly influence storm intensity.

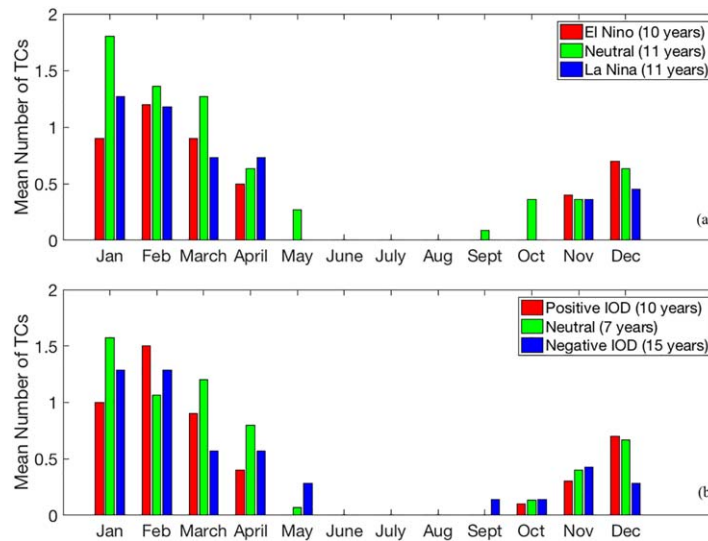


Figure 11. (a) Mean number of TCs in the SWTIO from 1981 to 2013 during each phase of ENSO for each month of a year, and (b) Mean number of TCs in the SWTIO from 1981 to 2013 during positive, negative, and neutral IOD events.

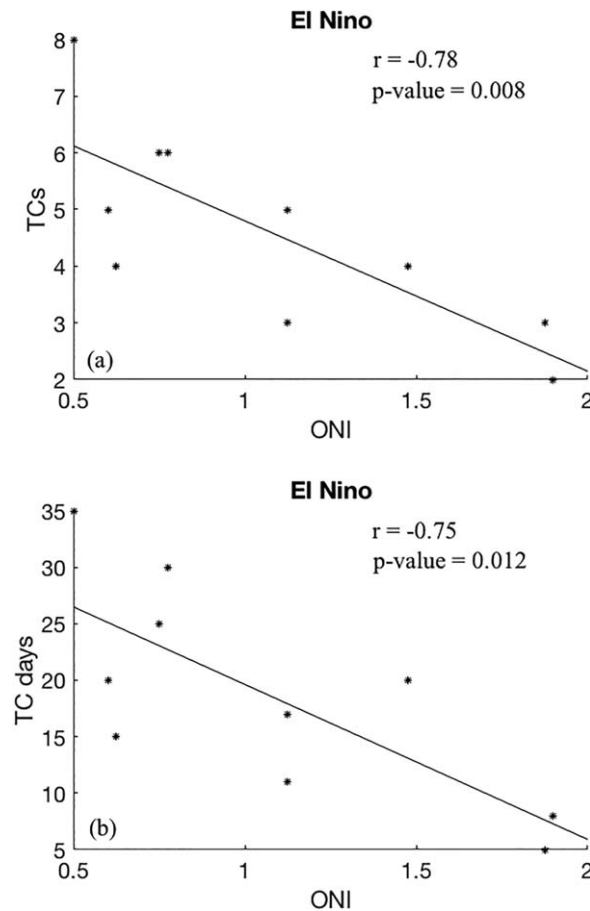


Figure 12. Scatter plots showing the relationships (top) between ONI versus number of TCs and (bottom) between Oceanic Niño Index (ONI) versus TC days for positive ENSO phase years between 1981 and 2013.

3.3. Role of ENSO and IOD Events on the SWTIO Cyclonic Activity

Preexisting studies have been done to examine TC activity over the SWTIO. However, the use of different data sets have resulted in varying results amongst these studies. A recent study by *Astier et al.* [2015] used primarily TC data from the Meteo-France RSMC La Réunion database. However, when a TC was included in the JTWC database and not in the RSMC's database, *Astier et al.* [2015] added that TC to their database. *Astier et al.* [2015] used the years 1981–2013 as their study period and excluded all TCs in the Mozambique Channel arguing that TC activity in this area may be different than

TC activity in the rest of the SWTIO. They also focused only on peak TC season months (January–March). We obtained our TC data from the JTWC database for 1981–2013. We considered the entire SWTIO (some Mozambique Channel TC eventually cross into the main SWTIO region and vice versa) and considered the entire TC season since some of the most intense TC cyclones occur outside of the peak TC months.

Since there are different numbers of El Niño (10 years total), La Niña (11 years total) and Neutral years (11 years total) during the 1981–2013 time period, we standardized the data by subtracting the long-term mean (mean for 1981–2013 period) from the mean of each ENSO phase and dividing by the long-term standard deviation (standard deviation for 1981–2013 period). Both the number of TCs and TC days were plotted to see if there was a difference between the number of TCs and the duration the TCs were lasting. During neutral years, the mean number of TCs and the mean number of TC days is approximately 0.7 standard deviations above the long-term total mean of TC (Figure 10). Both El Niño and La Niña years experience below average number of TCs and TC days (Figure 10). In addition to more cyclones occurring during the neutral years, the TC season also lasted longer and began earlier during neutral years as well. During the

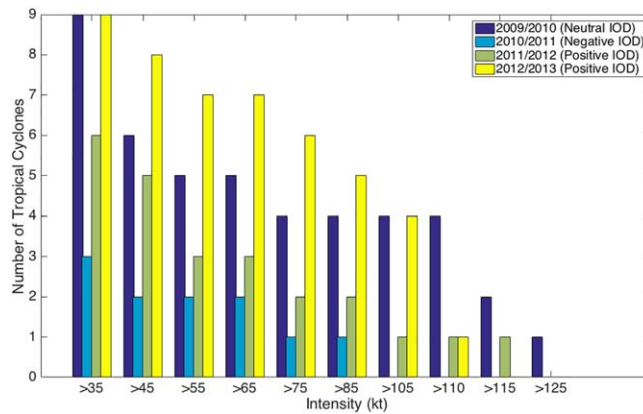


Figure 13. Intensity versus Number of Tropical Systems in the SWTIO for 4 IOD events and corresponding TC seasons.

months of September, October and May the TCs occurred during neutral years (Figure 11a) but not during years of positive or negative ENSO phase. However, this may also be a result of a 1 year smaller sample size for El Niño years during our study period or simply too small of sample sizes for all three categories to be statistically accurate.

With regard to the neutral phase of ENSO, *Astier et al.* [2015] concluded that neutral years seem to have high variability in TC activity. Although the TC days may be variable during these years, more TC days do still occur during

neutral years in comparison to the positive and negative phases of ENSO (Figure 10). While they concluded that cyclogenesis seems to be less favored during La Niña years, we also conclude that there seems to be less TC activity during La Niña years. For the positive ENSO phase, *Astier et al.* [2015] concluded that there is competition between favorable and unfavorable conditions for cyclogenesis. During El Niño years, cyclogenesis would be favored because of higher SST, higher humidity, and vorticity [*Kuleshov et al.*, 2009]. However, the equator-ward shift of the subtropical jet creates wind shear, which can suppress the storm formation, in the areas where TCs typically form (10° – 20° S) [*Heureux and Thompson*, 2006]. Although they noted low TC activity being associated with El Niño years, overall their study concluded that there is no clear linear relationship between ENSO and TC activity. However, when looking at just the positive phase of ENSO, we do see a statistically significant correlation between the positive phase of ONI and the number of TCs ($r = -0.78$, $p = 0.008$) and TC days ($r = -0.75$, $p = 0.012$) (Figure 12). As the ONI index increases, the number of TCs and TC days decreased.

There seems to be a less clear pattern with regard to IOD events and the mean number of TCs each month (Figure 10b). Some months, years of positive IOD events have the largest mean number of TCs while other months' neutral or negative IOD years seem to (Figure 10b). These inconsistent results may be due to the timing of the downwelling and upwelling Rossby waves (associated with IOD events) reaching the SCTR region. On the other hand, it could be due to skewed data since the sample size for the positive IOD, neutral, and negative IOD are different.

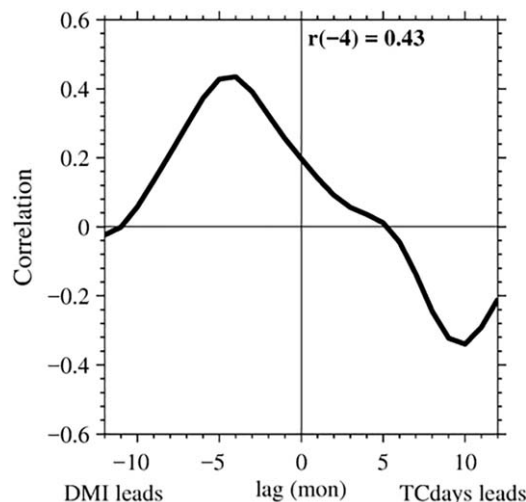


Figure 14. Lead-lag correlation plot between the DMI and TC days where the DMI and TC days between 2003 and 2013 are correlated against each other at zero lag and then at subsequent month lags.

With regard to intensity, we also do not observe any obvious pattern. The year 2012 was a positive IOD and we see the highest number of storm systems for most of the intensity categories during the 2012/2013 TC season (Figure 13). However, the year 2011 was also a positive IOD and this was not the case. A difference in the strength or the peak month of the IOD events may have resulted in the inconsistent results for those 2 years. The 2010 negative IOD year showed the least amount of tropical systems for each of the intensity categories and also produced no TCs with an intensity greater than 43 m/s or 85 kt (Figure 13). However, to draw the conclusion that negative IOD events result in less intense TCs, more negative IOD years data would be needed for the analysis.

With regard to the intensity of the IOD event and TC activity, there seems to be no direct correlation between the DMI of a year and the number of TC days in the same year (figure not shown). However, a 4–5 month lag relationship exists between the

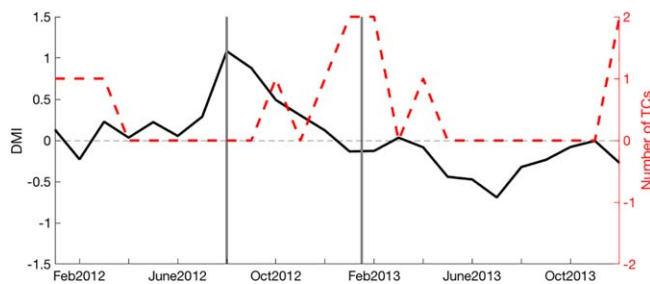


Figure 15. Dipole Mode Index (DMI, black line) and Number of TCs each month (red dashed line) for the years 2012 and 2013. The first vertical gray line represents the peak DMI of the 2012 IOD. The second vertical gray line represents the peak number of TCs during TC season.

DMI of a year and the number of TC days (Figure 14). In Figure 14, the DMI and TC days during 2003 and 2013 are correlated against each other at zero lag and then at subsequent month lags. The DMI of 2012 would be setting the stage for the 2012/2013 cyclone season, with a 4–5 months lag between the peak DMI for 2012 (August–September) and the peak in TC season (January–February 2013) (Figure 15). This lag is due to the approximate time it takes for downwelling Rossby waves generated

at the periphery of the colder SST band off southern Sumatra coast during positive IOD events to propagate westward across the SWTIO ocean basin. It takes approximately 4–6 months for downwelling Rossby waves to reach about 60–80°E (the region where most TCs form in the SWTIO, Figure 3).

4. Summary and Conclusions

In this study, we examined how phenomena like IOD and ENSO events impact the variability of TCs in the SWTIO. We found that there seems to be a negative linear correlation between the positive phase of ENSO and TC days in the SWTIO while neutral ENSO years seem to have more TC activity than other years. We also analyzed how Rossby waves associated with IOD events may influence BL and thus TCs. The BLT was correlated to atmospheric conditions important for cyclogenesis over a 4 year period and results showed that during this 4 year period midtropospheric instability and vertical wind shear values that may be unfavorable to TCs are associated with thicker BLs favoring TC formation. The BLT along the cyclone tracks were also studied to see if the BL along the cyclone tracks could influence the storm intensity. However, the large variability between these results suggested that the BLT alone does not significantly influence storm intensity.

In summary, we examined the relationship between the properties of the SCTR region and TCs in the SWTIO, while focusing on the 2012/2013 TC season. The year 2012 was a positive IOD year and a neutral ENSO year. In the SWTIO, on average, neutral years experienced higher number of TCs. Therefore, the lack of an ENSO event in 2012 may have played a role in the number of TC days during that season. With regard to IOD, we established that there is a 4–5 month lag correlation between DMI index and number of TC days in the SWTIO region. This lag time is attributed to the traveling time of Rossby waves (4–6 months) across the IO basin to the SCTR region. Therefore, the occurrence of a positive Indian Ocean Dipole in 2012 possibly influenced the number of TC days in that season through downwelling Rossby waves. As the Rossby waves propagated westward, they deepened the thermocline and thickened the BL resulting in enhanced warming at the surface, and increased cyclogenesis in early 2013. Although we now have a better understanding of the dynamics that influenced the active 2012/2013 TC season, still more research is needed to see if these findings hold true for other seasons as well. In addition, other impact of these climate phenomena (beyond the enhancement of surface warming) and their relation to TCs also needs to be explored.

References

Annamalai, H., R. Murtugudde, J. Potemra, S.-P. Xie, P. Lui, and B. Wang (2003), Coupled dynamics over the Indian Ocean: Spring initiation of the zonal mode, *Deep Sea Res., Part II*, 50, 2305–2330.

Astier, N., M. Plu, and C. Claud (2015), Association between tropical cyclone activity in the Southwest Indian Ocean and El Niño Southern Oscillation, *Atmos. Sci. Lett.*, 16, 506–511, doi:10.1002/asl.589.

Balaguru, K., P. Chang, R. Saravanan, L. R. Leung, Z. Xu, M. Li, and J. Hsieh (2012), Ocean barrier layers' effect on tropical cyclone intensification. *Earth Atmos. Planet. Sci.*, 109, 14343–14347, doi:10.1073/1201364109.

Bleck, R. (2002), An oceanic general circulation model framed in hybrid isopycnic-Cartesian coordinates, *Ocean Modell.*, 4(1), 55–88.

Chassignet, E. P., L. T. Smith, G. R. Halliwell, and R. Bleck (2003), North Atlantic simulations with the HYbrid Coordinate Ocean Model (HYCOM): Impact of the vertical coordinate choice, reference pressure, and thermobaricity, *J. Phys. Oceanogr.*, 33(12), 2504–2526.

Chowdary, J. S., C. Gnanaseelan, and S. P. Xie (2009), Westward propagation of barrier layer formation in the 2006–07 Rossby wave event over the tropical southwest Indian Ocean, *Geophys. Res. Lett.*, 36, L04607, doi:10.1029/2008GL036642.

Acknowledgments
This work is supported by the ONR Physical Oceanography Program Award #N00014-15-1-2591 awarded to BS. VSNM, is thankful to the Director of the CSIR-NIO for his keen interest in the joint-collaborative research with BS at the University of South Carolina, Columbia, USA. Joint Typhoon Warning Center (JTWC) best track data set for the Southern Hemisphere were obtained from http://www.usno.navy.mil/NOOC/nmfc-ph/RSS/jtbc/best_tracks/shindex.php. Argo data were obtained from the Asia-Pacific Data Research Center (APDR) of the International Pacific Research Centre (IPRC) (<http://apdr.csoest.hawaii.edu/las/v6/dataset?catitem=2>). Heat content data were obtained from https://www.nodc.noaa.gov/OC5/3M_HEAT_CONTENT/basin_data.html. ECMWF data sets were obtained from the ECMWF ERA-Interim data server. ERA-Interim Project, Monthly Means were obtained from NCAR Research Data Archive server. We would like to thank AVISO for making Sea Surface Height (SSH) data freely available. HYCOM simulations were provided by Dr. Jay F. Shriver, Naval Research Laboratory, Stennis Space Center, Mississippi. The authors would like to thank the anonymous reviewers, whose comments significantly contributed to the improvement of this paper. This has the NIO contribution 5928.

- Chu, J.-H., C. R. Sampson, A. S. Levine, and E. Fukada (2002), The Joint Typhoon Warning Center tropical cyclone best-tracks, 1945 – 2000, *Ref. NRL/MR/7540-02-16*, Nav. Res. Lab., Washington, D. C.
- Cummings, J. A. and O. M. Smedstad (2013), Variational data assimilation for the global ocean, in *Data Assimilation for Atmospheric, Oceanic and Hydrologic Applications*, edited by S. K. Park and L. Xu, vol. II, chap. 13, pp. 303–343, Springer-Verlag, Berlin Heidelberg, doi:10.1007/978-3-642-35088-7_13.
- Ducet, N., P.-Y. Le Traon, and G. Reverdin (2000), Global high resolution mapping of ocean circulation from TOPEX/Poseidon and ERS-1/2, *J. Geophys. Res.*, *105*, 19,477–19,498.
- Felton, C. S., B. Subrahmanyam, V. S. N. Murty, and J. F. Shriver (2013), ENSO-Modulated Cyclogenesis over the Bay of Bengal, *J. Clim.*, *26*, 9806–9818, doi:10.1002/2013JC009759.
- Felton, C. S., B. Subrahmanyam, V. S. N. Murty, and J. F. Shriver (2014), Estimation of the barrier layer thickness in the Indian Ocean using Aquarius Salinity, *J. Geophys. Res. Oceans*, *119*, 4200–4213, doi:10.1002/2013JC009759.
- Gnanaseelan, C., B. H. Vaid, and P. S. Polito (2008), Impact of biannual Rossby Waves on Indian Ocean dipole, *IEEE Geosci. Remote Sens. Lett.*, *5*, 427–429.
- Gray, W. M. (1968), Global view of the origin of tropical disturbances and storms, *Mon. Weather Rev.*, *96*, 669–700.
- Gray, W. M. (1979), Hurricanes: Their formation, structure and likely role in the tropical circulation, in *Meteorology over Tropical Oceans*, edited by D. B. Shaw, pp. 155–218, R. Meteorol. Soc., Bracknell, U. K.
- Halkides, D., and T. Lee (2011), Mechanisms controlling seasonal-to-interannual mixed layer temperature variability in the southwestern tropical Indian Ocean, *J. Geophys. Res.*, *51*, 77–93, doi:10.1016/j.jdynatmoce.2011.03.002.
- Hermes, J. C., and C. J. C. Reason (2009a), Annual cycle of the South Indian Ocean (Seychelles-Chagos) thermocline ridge in a regional ocean model, *J. Geophys. Res.*, *114*, C02012, doi:10.1029/2008JC004949.
- Hermes, J. C., and C. J. C. Reason (2009b), The sensitivity of the Seychelles-Chagos thermocline ridge to large scale wind anomalies, *ICES J. Mar. Sci.*, *66*, 1455–1466.
- Hoffman, G. F., D. T. Bolvin, E. J. Nelkin, D. B. Wolff, R. F. Adler, G. J. Gu, Y. Hong, K. P. Bowman, and E. F. Stocker (2007), The TRMM Multi satellite Precipitation Analysis (TMPA): Quasi-global, multiyear, combined-sensor precipitation estimates at fine scales, *J. Hydrometeorol.*, *8*, 38–55.
- Kuleshov, Y. F., Chane, L. Qi, I. Chouaibou, C. Hoareau, and F. Roux (2009), Tropical cyclone genesis in the Southern Hemisphere and its relationship with ENSO, *Ann. Geophys.*, *27*, 2523–2538.
- Levitus, S., et al. (2012), World ocean heat content and thermosteric sea level change (0–2000 m), 1955–2010, *Geophys. Res. Lett.*, *39*, L10603, doi:10.1029/2012GL051106.
- L’Heureux, M.L. and D.W. J. Thompson (2006), Observed relationships between the El Niño Southern Oscillation and the extratropical zonal-mean circulation, *J. Clim.*, *19*, 276–287.
- Mainelli, M., M. DeMaria, L. K. Shay, and G. Goni (2008), Application of oceanic heat content estimation to operational forecasting of recent Atlantic Category 5 hurricanes, *Weather Forecasting*, *23*, 3–16, doi:10.1175/2007WAF2006111.1
- Manola, I., F.M. Selten, W. P. M. de Ruijter, and W. Hazeleger (2015), The ocean atmosphere response to wind-induced thermocline changes in the tropical South Western Indian Ocean, *Clim. Dyn.*, *45*, 989–1007, doi:10.1007/s00382-014-2338-7.
- McCreary, J. P., P. K. Kundu, and R. L. Molinari (1993), A numerical investigation of dynamics, thermodynamics and mixed-layer processes in the Indian Ocean, *Prog. Oceanogr.*, *31*, 181–244.
- Metzger, E. J., et al. (2014), US Navy operational global ocean and Arctic ice prediction systems, *Oceanography*, *27*(3), 32–43.
- RSMC (2015), Review of recent (2012–2015) main activities and achievements at RSMC La Reunion, edited by *RSMC La Réunion*, pp 1–8, World Meteorological Organization (WMO), Geneva, Switzerland.
- Saji, N. H., B. N. Goswami, P. N. Vinayachandran, and T. Yamagata (1999), A dipole mode in the tropical Indian Ocean, *Let. Nat.*, *401*, 360–363.
- Sampson, C. R., and A. J. Schrader (2000), The Automated Tropical Cyclone Forecasting System (Version 3.2), *Bull. Amer. Meteor. Soc.*, *81*, 1131–1240.
- Vialard, J., et al. (2009), Cirene: Air-sea interactions in the Seychelles-Chagos thermocline ridge region, *Bull. Am. Meteorol. Soc.*, *90*, 45–61, doi:10.1175/2008BAMS2499.1.
- Vinayachandran, P. N., P. A. Francis, and S. A. Rao (2009), Indian Ocean Dipole: Processes and impacts, *Indian Acad. Sci. Platinum Jubilee*, *P1*, 1–21.
- Wolter, K., and M. S. Timlin (1993), Monitoring ENSO in COADS with a seasonally adjusted principal component index, in *Proceedings of the 17th Climate Diagnostics Workshop*, pp. 52–57, NOAA/NMC/CAC, NSSL, Okla. Clim. Surv., CIMMS and the Sch. of Meteorol., Univ. of Okla., Norman.
- Wolter, K., and M. S. Timlin (1998), Measuring the strength of ENSO events – how does 1997/98 rank?, *Weather*, *53*, 315–324.
- Xie, S. P., H. Annamalai, F. A. Schott, and J. P. McCreary Jr. (2002), Structure and mechanism of South Indian Ocean climate variability, *J. Clim.*, *15*, 864–878.